Journal of Mining and Earth Sciences

Website: https://jmes.humg.edu.vn

A numerical workflow for sand production prediction accounting for stresses redistribution around perforation tunnels: insights from well A-1P, Cuu Long basin

Hoang Van Nguyen [1,*], Huong Thien Phan [2], Vinh The Nguyen [2]

[1] Petrovietnam Exploration and Production Corporation, Hanoi, Vietnam
[2] Hanoi University of Mining and Geology, Hanoi, Vietnam

ARTICLE INFO

Article history:
Received 20th Apr. 2026
Revised 08th Jul. 2026
Accepted 17th Jul. 2026

Keywords:
Critical,
Cuu Long Basin,
Drawdown,
Load Factor,
Pressure (CDP),
Sand production prediction.

ABSTRACT

Sand production is a phenomenon in which disintegrated sand grains are carried with fluid flow from formation, leading to equipment erosion, reduced productivity, and significant economic losses. Conventional sand production prediction typically computes stresses at the wellbore, frequently neglecting stress redistribution around perforation tunnels.

To address this gap, this paper utilized a Python-based numerical script to compute the maximum effective tangential compressive stress ($\sigma_{\theta 1max}$) by solving borehole stress equations across a 360^0 circumferential range for various perforation angles (0^0, 30^0, 60^0 and 90^0). Concurrently, a continuous thick-walled cylinder (TWC) strength profile along the wellbore generated by using an empirical correlation between core laboratory tests and log-derived uniaxial compressive strength (UCS). Both parameters serve as critical inputs for the Load Factor (LF) criterion which was applied to identify sand-prone intervals and determine the Critical Drawdown Pressure (CDDP).

The model was validated against field production data from the perforated interval 1817÷1823.6 mMD, which flowed 928 BOPD and 5.74 MMscf/day. The prediction results showed interbedded sanding and sand-free zones, confirming that sand production could occur under most drawdown conditions. The result is highly consistent with the number of sand grains counted at the surface from the early production stage. In addition, the sensitivity analysis showed that reservoir pressure depletion significantly impacts sand production. The study aims to provide a robust framework for sand production management in Field X. The integration of geomechanical modeling with real-time production data allows for the optimization of well trajectories and perforation orientations, effectively minimizing sanding risks and maximizing the economic life cycle of the well.

*Corresponding author
E - mail: hoangnv@pvep.com.vn
DOI: 10.46326/JMES.2026.67(4).10

1. Introduction

Sand production is a phenomenon in which disintegrated sand grains are carried with fluid flows from formation. These solid grains can cause significantly economic losses and compromises the safe operation of the oil and gas fields. Therefore, it is essential to develop a sand production prediction model to mitigate sanding issues in the wellbores.

To mitigate the effect of sanding problem, various sand-control techniques have been applied, including gravel-pack completion, sand-screen, which can filter sand grains from the produced fluid. However, these methods are often expensive and technically challenging to implement. Currently, the application of sand production model has become increasingly common. These models utilize geomechanical parameters derived from the well logs and integrate with core analysis to optimize well trajectory, perforated orientation, proposal of drawdown and sand production prediction. Initially, Khamehchi & Reisi (2015) proposed a method for predicting sand production based on the ratio of shear modulus to bulk compressibility. Wu et al. (2010), Rahman et al. (2010), Dung et al. (2014) Duyen et al. (2024), and Asadi et al. (2016) proposed a geomechanical models based on wireline logging data to estimate pore presure, overburden stress, and rock strengths. However, these studies mainly address sand production related to wellbore stresses and rarely mention the stress changes occurring around the walls of perforation tunnels.

To apply the sand production prediction model, Well A-1P was selected from Field X, Block Y, in the Cuu Long Basin, located approximately 160 km east of Vung Tau. Binh et al. (2007, 2011) characterized the stress regime in the Cuu Long Basin as being dominated by a normal faulting stress regime. The primary targets are the Miocene reservoirs, which consist predominantly of sandstones and claystones interbedded with thin volcanic layers.

In this paper, a model for stress distributions around a perforation tunnel was proposed using a cylindrical coordinate system (Wang et al., 2022). The output of this geomechanical model, specifically the redistributed stress state around the wall of the perforation tunnel, was then incorporated into a failure assessment using the Load Factor (LF) criterion. Based on this theoretical framework, a Python-based numerical script was developed to solve the complex stress equations over a full 360^0 circumferential domain. This allows for the precise calculation of LF for various perforation angles (0^0, 30^0, 60^0, and 90^0) and the determination of reliable critical drawdown pressures (CDP) under different reservoir depletion scenarios (0%, 15%, 30%, and 35% depletion). The model was validated against both laboratory core tests and real-time production data. The results aim to provide a reliable framework for optimizing drawdown strategies and ensuring sand-free production throughout the life cycle of the reservoir and avoiding production from sand-prone intervals.

2. Database of study area and sand-failure criterion

2.1. Database of study area

In this study, data from Well A-1P in Field X, Block Y of the Cuu Long Basin were used to predict sand production. The dataset includes gamma ray (GR, API), deep/shallow resistivity (LLD/LLS, and Ohm·m), density (RHOB, g/cm^3), neutron porosity (NPHI, etc.), and compressional/shear slowness logs (DTC/DTS, μs/ft). The main targets in these wells are the oil-bearing sandstone intervals of the Miocene and Oligocene sequences. In particular, one of the most important parameters is the thick-walled cylinder (TWC) strength, derived from core tests, which is used to calibrate and validate log-derived TWC estimates.

2.2. Sand-failure Criteria

Sand-failure criteria are established based on the shear-failure mechanism induced by stress redistribution. These stress changes affect the walls of the perforation tunnels as the internal wellbore pressure varies in response to the changes in flowing pressure. Consequently, these criteria determine the allowable drawdown pressure and the associated stress thresholds required to maintain sand-free production throughout the life of the well.

To analyze and calculate the stresses surrounding perforation tunnels, it is necessary to utilize and transform between three distinct coordinate systems (Fraer et al., 2008; Zoback, 2007; Wang et al., 2022). Figure 1 illustrates the stress distribution with respect to geographic, principal stress, and cylindrical coordinate system for both an arbitrary oriented trajectory well and its perforated tunnels. Within the cylindrical system, the stress state is resolved into radial,

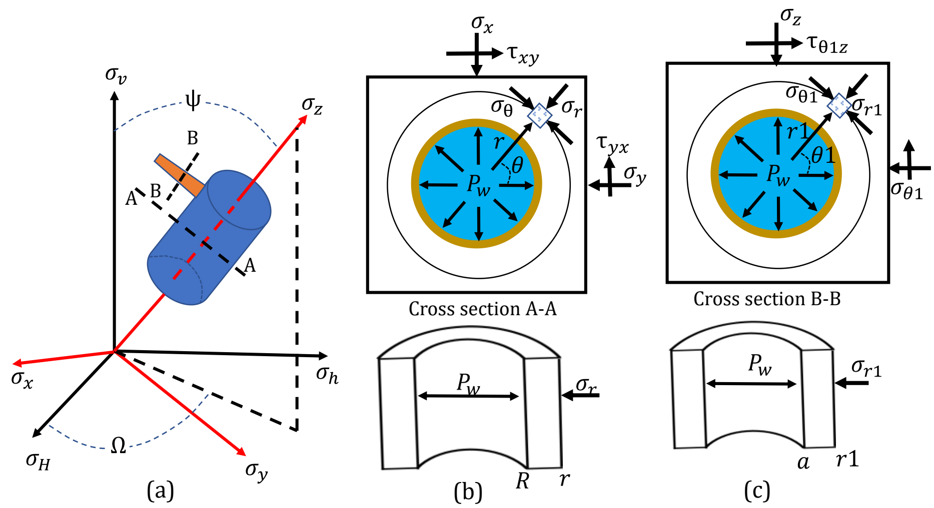

Figure 1. (a), (b) Stresses distribution around the wellbore expressed in principal, Cartersian and cylindrical coordinate system. (c) Stress distribution around perforated tunnels expressed in the cylindrical coordinate system.

circumferential, and axial stress components around the wellbore and perforation walls, respectively. In the case of vertical well, the pricipal stress coordinate system concides with geographic coordinate system.

The in-situ stress state in a sedimentary basin includes the minimum horizontal stress(σ_h), maximum (σ_H) horizontal stress and overburden (σ_v) stress. The magnitude and relative order of these stresses depend on the tectonic regime, which is classified according to Andersonian fault theory. (Binh et al., 2007) classified the stress regime of the Cuu Long Basin as a normal faulting regime, where $\sigma_v > \sigma_H > \sigma_h$. The horizontal stresses σ_H, σ_h can be calculated using the equations as below (Zain-Ul-Abedin, 2020):

$$\sigma_h = \frac{\vartheta}{1-\vartheta}\sigma_v + \frac{1-2\vartheta}{1-\vartheta}\alpha P_p + \frac{E}{1-\vartheta^2}\varepsilon_h + \frac{\vartheta E}{1-\vartheta^2}\varepsilon_H \quad (1)$$

$$\sigma_H = \frac{\vartheta}{1-\vartheta}\sigma_v + \frac{1-2\vartheta}{1-\vartheta}\alpha P_p + \frac{E}{1-\vartheta^2}\varepsilon_H + \frac{\vartheta E}{1-\vartheta^2}\varepsilon_{min} \quad (2)$$

σ_h - Minimum horizontal stress, psi; σ_H - Maximum horizontal stress, psi; ϑ: Static Poisson ratio, unitless; E- Static Young's module, psi; P_p- Formation pore pressure, psi; α - Biot's constant, equals to 1; $\varepsilon_h, \varepsilon_H$- indexes of horizontal tension and define by calibration with leak of test values.

Figure 1a, the in-situ stress components expressed in the Cartesian coordinate system of the wellbore are given as follows (Fraer et al., 2008; Zoback, 2007; Rahman et al., 2010; Wang et al., 2022):

$$\sigma_x = (\sigma_H cos^2\Omega + \sigma_h sin^2\Omega)cos^2\Psi + \sigma_v sin^2\Psi \quad (3)$$

$$\sigma_y = \sigma_H sin^2\Omega + \sigma_h cos^2\Omega \quad (4)$$

$$\sigma_z = (\sigma_H cos^2\Omega + \sigma_h sin^2\Omega)sin^2\Omega + \sigma_v cos^2\Omega \quad (5)$$

$$\tau_{xy} = -0.5(\sigma_H - \sigma_h)sin2\Omega cos\Psi \quad (6)$$

$$\tau_{yz} = -0.5(\sigma_H - \sigma_h)sin2\Omega sin\Psi \quad (7)$$

$$\tau_{xz} = 0.5(\sigma_H cos^2\Omega + \sigma_h sin^2\Omega - \sigma_v)sin\Psi \quad (8)$$

Where $\sigma_x, \sigma_y, \sigma_z, \tau_{xy}, \tau_{yz}, \tau_{xz}$ are in situ stress components at the Cartersian coordinates, psi. Ω is the azimuth angle of wellbore, degree. Ψ is the inclination of wellbore, degree.

The stress distribution around wall of wellbore is given in the cylindrical coordinate system as below:

$$\sigma_r = \left(\frac{\sigma_x+\sigma_y}{2}\right)\left(1-\frac{R^2}{r^2}\right) + \left(\frac{\sigma_x-\sigma_y}{2}\right)\left(1+3\frac{R^4}{r^4}-4\frac{R^2}{r^2}\right)cos2\theta + \tau_{xy}\left(1+3\frac{R^4}{r^4}-4\frac{R^2}{r^2}\right)sin2\theta + (P_r-P_w)\frac{R^2}{r^2} \quad (9)$$

$$\sigma_\theta = \left(\frac{\sigma_x+\sigma_y}{2}\right)\left(1+\frac{R^2}{r^2}\right) - \left(\frac{\sigma_x-\sigma_y}{2}\right)\left(1+3\frac{R^4}{r^4}\right)cos2\theta - \tau_{xy}\left(1+3\frac{R^4}{r^4}\right)sin2\theta - A(P_r-P_w)\frac{R^2}{r^2} \quad (10)$$

$$\sigma_z = \sigma_z - \upsilon[2(\sigma_x-\sigma_y)\frac{R^2}{r^2}cos2\theta + 4\tau_{xy}\frac{R^2}{r^2}sin2\theta] \quad (11)$$

$$\tau_{r\theta} = \left(\frac{\sigma_x-\sigma_y}{2}\right)\left(1-3\frac{R^4}{r^4}+2\frac{R^2}{r^2}\right)sin2\theta + \tau_{xy}\left(1-3\frac{R^4}{r^4}+4\frac{R^2}{r^2}\right)cos2\theta \quad (12)$$

$$\tau_{\theta z} = (-\tau_{xz}sin\theta + \tau_{yz}cos\theta)(1+\frac{R^2}{r^2}) \quad (13)$$

$$\tau_{rz} = (-\tau_{xz}cos\theta + \tau_{yz}sin\theta)(1+\frac{R^2}{r^2}) \quad (14)$$

The borehole with assumption of R=r, which mean that the stresses at the wall of wellbore are equated to:

$$\sigma_r = (P_r - P_w) \quad (15)$$

$$\sigma_\theta = \sigma_x + \sigma_y - 2(\sigma_x-\sigma_y)cos2\theta + 4\tau_{xy}sin2\theta - A(P_w - P_r) \quad (16)$$

$$\sigma_z = \sigma_z - \upsilon[2(\sigma_x-\sigma_y)cos2\theta + 4\tau_{xy}sin2\theta] \quad (17)$$

$$\tau_{r\theta} = 0 \quad (18)$$

$$\tau_{\theta z} = 2(-\tau_{xz}sin\theta + \tau_{yz}cos\theta) \quad (19)$$

$$\tau_{rz} = 0 \quad (20)$$

Where σ_r, σ_θ, σ_z .(Figure 1b) are the radial, hoop and axial stresses in cylindrical coordinate, respectively, psi; $\tau_{\theta z}$, $\tau_{r\theta}$, τ_{rz} are shear stress in cylindrical coordinate, psi; θ - wellbore circumferential angle, degree; υ - Poisson's ratio. P_r - the reservoir pressure, psi; P_w - mud pressure, psi; r - radial distance, m; R - radius of wellbore, m.

The perforated tunnels can be considered a micro open-hole well connected to and is perpendicular to the wellbore (Figure 1c). The fluid inside the tunnels and stress components act together on the rock around the tunnels. The stress components for perforated tunnels can be expressed in the cylindrical coordinate system r_1, θ_1, z_1 (Ding et al., 2017; Wang et al., 2022):

$$\sigma_{r1} = \left(\frac{\sigma_\theta+\sigma_z}{2}\right)\left(1-\frac{a^2}{r1^2}\right) + \left(\frac{\sigma_\theta-\sigma_z}{2}\right)\left(1+3\frac{a^4}{r1^4}-4\frac{a^2}{r1^2}\right)cos2\phi + \tau_{xy}\left(1+3\frac{a^4}{r^4}-4\frac{a^2}{r^{12}}\right)sin2\phi + (P_r-P_w)\frac{a^2}{r1^2} \quad (21)$$

$$\sigma_{\theta 1} = \left(\frac{\sigma_\theta+\sigma_z}{2}\right)\left(1+\frac{a^2}{r1^2}\right) - \left(\frac{\sigma_\theta-\sigma_z}{2}\right)\left(1+3\frac{a^4}{r1^4}\right)cos2\phi - \tau_{\theta r}\left(1+3\frac{a^4}{r1^4}\right)sin2\phi - (P_r-P_w)\frac{a^2}{r1^2} \quad (22)$$

$$\sigma_{z1} = \sigma_z - \upsilon[2(\sigma_\theta-\sigma_z)\frac{a^2}{r1^2}cos2\phi + 4\tau_{\theta r}\frac{a^2}{r1^2}sin2\phi] \quad (23)$$

$$\tau_{r\theta 1} = \left(\frac{\sigma_\theta-\sigma_z}{2}\right)\left(1-3\frac{R^4}{r1^4}+2\frac{a^2}{r1^2}\right)sin2\phi + \tau_{\theta z}\left(1-3\frac{a^4}{r1^4}+2\frac{a^2}{r1^2}\right)cos2\phi \quad (24)$$

$$\tau_{\theta 1z} = (-\tau_{r\theta}sin\phi + \tau_{rz}cos\phi)(1+\frac{a^2}{r^2}) \quad (25)$$

$$\tau_{r1Z} = (\tau_{rz}sin\phi + \tau_{r\theta}cos\phi)(1-\frac{a^2}{r1^2}) \quad (26)$$

Where ϕ is perforation circumferential angle, degree; $r1$ is the radial distance from the axis of the perforation tunnel, m; a is the radius of perforation tunnel, m. σ_{r1}, $\sigma_{\theta 1}$, σ_z are the radial stress, circumferential stress and axial stress respectively, resulting from the combined effects of perforation tunnel fluid pressure and the stress component computed from Eq. (21÷26), and $\tau_{r\theta 1}, \tau_{r1Z}, \tau_{\theta 1z}$ are the corresponding shear stresses, psi.

One sanding criterion is that sand grains become disaggregated due to shear failure when the maximum tangential effective compressive stress $\sigma_{e,max}$ exceeds the formation rock strength, U (Rahman et al., 2010; Asadi et al. 2016; Willson et al., 2002; Banerjee et al., 2020). LF denotes the load factor.

$$\sigma_{e,max} \geq U \ or \frac{\sigma_{e,max}}{TWC*ESF} = LF \geq 1 \quad (27)$$

Thus, the well will be onset of sand production when $LF \geq 1$

The effective formation strength is defined as $U = TWC * ESF$. Khaksar et al. (2009), Asadi et al. (2016) and Tran et al. (2025) proposed a relationship between Thick walled cylinder (TWC) from core laboratory core testing with porosity, or compressive slowness (DTC), or density (RHOB).

In this study, the authors integrated TWC and Unconfined Compressive Strength (UCS) core data from Well A-1P and nearby offset wells to establish an emperical correlation for predicting the TWC profile of Well A-1P, as illustrated in Figure 2.

$$TWC = 46.265 * UCS^{0.6204} \quad (28)$$

However, core test data are sparsely distributed and are not available as a continuous log profile. (Hoang, 2026) proposed a correlation

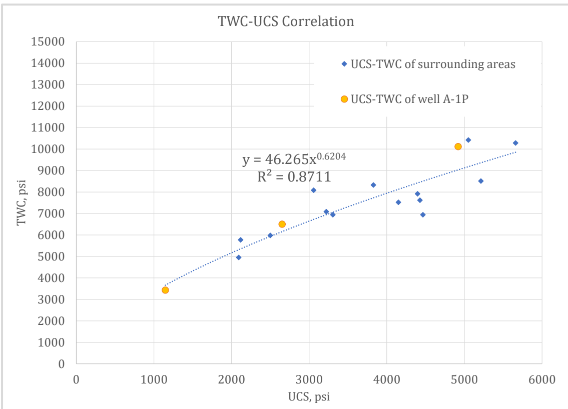

Figure 2. Correlation between UCS-TWC in Surrounding and Study areas.

between the P-wave modulus (M) and Uniaxial Compressive Strength (UCS), derived from hydraulic flow units (HFU), to generate a continuous TWC profile along the wellbore by using equation 28, as illustrated in column 8, Figure 3. The comparison between the log-derived TWC profile and measured core test values demonstrates good agreement and predictive capability. Consequently, the Mean Absolute Error (MAE), Mean Absolute Percentage Error (MAPE), and Root Mean Square Error (RMSE) were calculated as 959.35 psi, 11.85%, and 1323.3 psi, respectively.

The Effective Strength Factor (ESF) should be adjusted to match the observed sand-failure evidence in a well under specific drawdown conditions during field production. In the absence of field data, conservative ESF values ranging from 2.0 to 3.1 are generally used.

For an arbitrary trajectory, the principal stresses acting in a plane tangential to the wellbore wall are considered, and the maximum principle stress, σ_{max} (σ_r acting normal to the wellbore wall), which is responsible for sand failure is calculated as follows (Waters et al., 2016; Rahman et al., 2010; Ding et al., 2018):

$$\sigma_{max} = 0.5(\sigma_z + \sigma_{\theta 1} + \sqrt{(\sigma_z + \sigma_{\theta 1})^2 + 4\tau_{\theta 1 z}{}^2}) \quad (29)$$

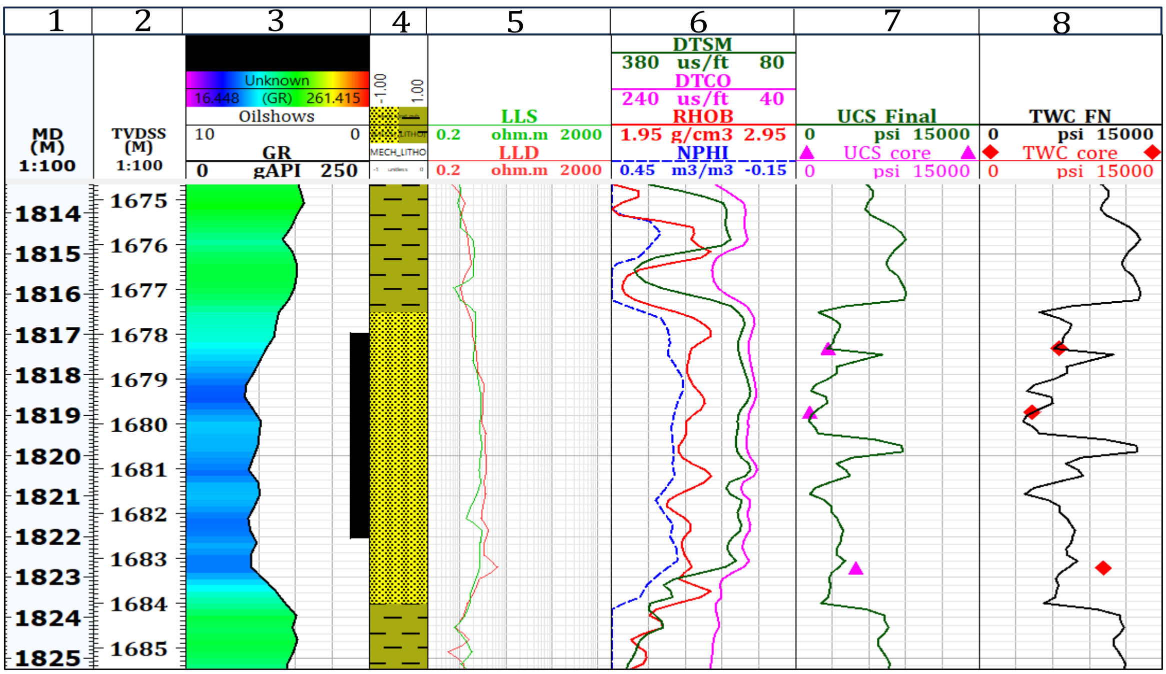

Figure 3. Wireline logging data and illustrations of correlation of log_derived UCS, TWC vs measured core test values.

The maximum effective tangential compressive stress, $\sigma_{e,max}$ - calculated as $\sigma_{max} - P_w$, where P_w - the wellbore pressure during production, which is usually known as the bottom hole flowing pressure (BHFP). In this paper the authors utilized a Python script to calculate σ_{max} by solving the equation (29) across a range of θ values, using small increments from 0÷360^0. These calculations were performed for perforation angles ($\boldsymbol{\phi}$) of 0^0, 30^0, 60^0, 90^0. The angle θ - defined as positive counterclockwise direction from the σ_H direction in a vertical well and from the top of the wellbore in an inclined hole).

Fuller et al. (2017) noted that as reservoir pressure decreases during production, the in-situ stress state within the reservoir changes, often resulting in variation in the magnitudes of the horizontal stresses. This stress redistribution leads to changes in the allowable drawdown, which can trigger sand failure. Consequently, these factors must be integrated into long-term sand production control strategies, alongside the management of Bottom Hole Flowing Pressure (BHFP) relative to the declining reservoir pressure. The Critical Drawdown Pressure (CDDP, psi) is defined as the pressure differential required to induce rock failure:

$$CDDP = \varDelta P - CBHP \qquad (30)$$

$$CBHP = \frac{3*\sigma_{\theta 1} - \sigma_{r1} - U}{2-A} - \varDelta P * \frac{A}{2-A} \qquad (31)$$

$CBHP$ - critical bottom hole pressure, psi; $\varDelta P$ - the difference between the depletion pressure and the initial pressure, psi; A - poro-elastic constant given by: $A = \frac{1-2\nu}{1-\nu}$; ν - poisson's ratio.

3. A case study: application to well A-1P, field X and discussion

A case study

This case study focuses on Well A-1P in Block Y of the Cuu Long Basin. Well A-1P is a production well featuring a high-deviation design, with a maximum inclination of 63^0. The Well A-1P was selected to investigate sand production risk within the main Mioccene producing reservoirs intervalbetween 1817÷1823.6 mMD. The well was completed as a cased-hole completion and produced 928 BOPD, and 5.74 Mmscf/d as shown in Table 1.

The results presented in Figure 4 describes the well profile across various tracks. Tracks 1 and 2 display the measured depth (MD) and total vertical depth subsea (TVDSS), respectively. Track 3 displays the oil-show interval, the Gamma Ray (GR) wireline log, and the GR measurement from logged core, demonstrating the depth shift applied to align the core data with the wireline logs. Track 4 illustrates the lithology, identifying sandstone and shale intervals. Tracks 5 and 6 exhibit good consistency between the log-derived UCS and TWC data and their corresponding core test results (represented by the black and red points in tracks 5 and 6). To evaluate the onset of sanding, three specific depths were selected for sensitivity analysis, labeled as Points 1, 2, and 3 in Figure 4. Within the production interval from 1817 to 1823.6 mMD, Track 8 illustrates the Critical Drawdown Pressure (CDDP) values corresponding to reservoir pressure depletion levels of 0%, 15%, 30%, and 35%. Analysis of the sub-intervals 1817÷1818 mMD, 1819.6÷1820.6 mMD, and 1821÷1822.9 mMD

Table 1. Database of well A-1P in study area.

Well	Formation	Log Depth (m)	GR (API)	LLD/ LLS (Ohmm)	RHOB (g/cm^3)	NPHI (Dec)	DTC/ DTS (μs/ft)	Core Interval (m)
A-1P	Miocene	1750÷2340	yes	yes	yes	yes	yes	1812.5÷1823.42

<table>
<tr><td colspan="4">Core Point Analysis</td><td colspan="5" rowspan="2">Production Test Results</td></tr>
<tr><td rowspan="5">A-1P</td><td>Depth (m)</td><td>UCS (psi)</td><td>TWC (psi)</td></tr>
<tr><td rowspan="2">1817.34</td><td rowspan="2">2651</td><td rowspan="2">6500</td><td colspan="2" rowspan="2">Perforation Interval (mMD)</td><td colspan="3">Flow rates</td></tr>
<tr><td>Oil (BOPD)</td><td>Gas (MMSCF/D)</td><td>Water (BWPD)</td></tr>
<tr><td>1818.92</td><td>1147</td><td>4269</td><td rowspan="2">1817</td><td rowspan="2">1823.6</td><td rowspan="2">928</td><td rowspan="2">5.74</td><td rowspan="2">Nil</td></tr>
<tr><td>1822.77</td><td>4919</td><td>10114</td></tr>
</table>

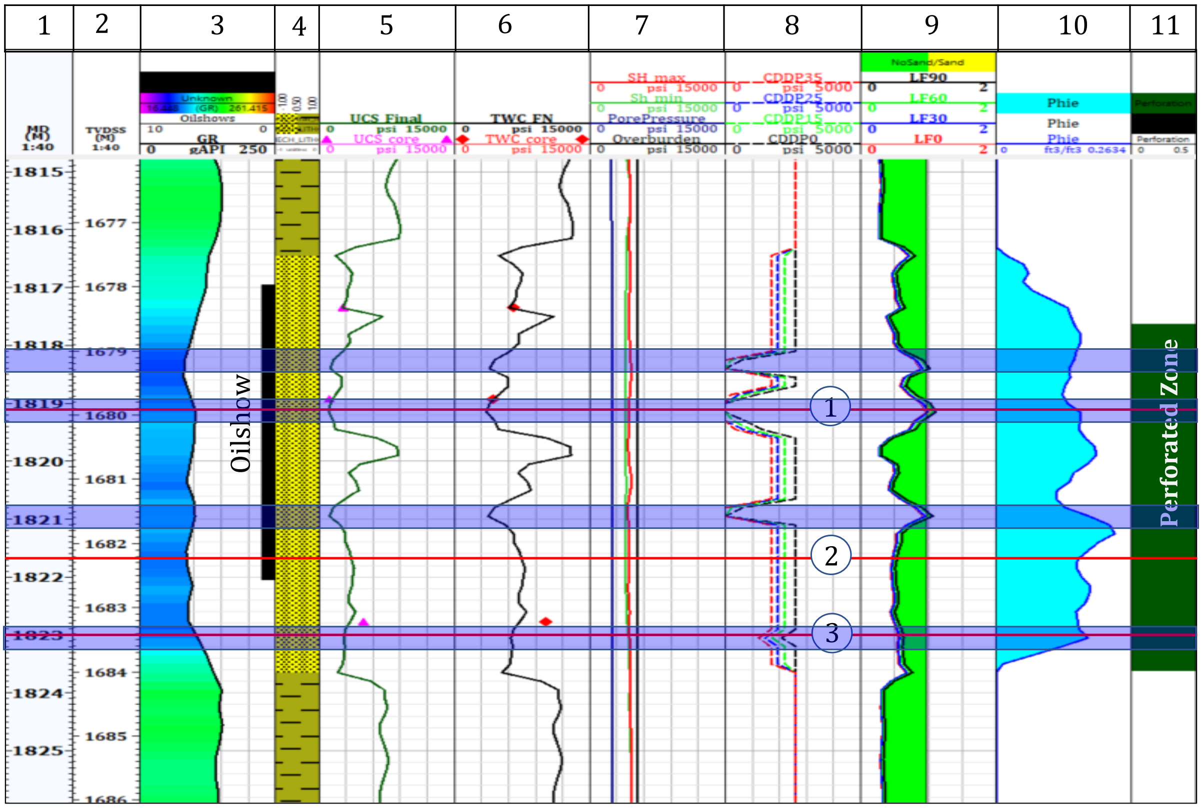

Figure 4. Sand production prediction highlights intervals with a high potential of sand production in the perforated interval in Well A-1P.

indicates that a drawdown pressure ranging from 2591÷1684 psi can be applied without sand production. Conversely, the intervals 1818.2÷1819.6 mMD, 1820.6÷1821.06 mMD, and 1822.9÷1823.2 mMD show a higher sand production risk under the same conditions. Finally, Track 9 displays the Load Factor (LF) values for various perforation angles ($0÷90^0$). Intervals where LF > 1 (highlighted by yellow crossover areas) are identified as potential sand production zones. As shown in Figure 4, the results highlights potential sand production intervals that are consistent with the CDDP and LF. In the Track 9, several intervals-specifically 1817.2÷1817.8 mMD, 1818.8÷1819.8 mMD, 1820.6÷1820.8 mMD, and 1822.8÷1823.2 mMD-exhibit LF > 1 across all perforation orientations, indicating a high risk of sand production. An exception is noted at the 1822.8-1823.2 mMD depth, where sand-free production is possible if the perforation orientation is kept below 60^0. Consequently, the remaining perforated intervals are expected to flow without sand production.

The sand production sensitivity analysis is based on a cross-plot of reservoir pressure and bottom hole flowing pressure with the X- and Y-axes representing the reservoir pressure and bottom-hole flowing pressure respectively, while the scale below X-axis represents reservoir pressure depletion rate. The sand production sensitivity analysis (Figure 5) indicates stable zones in green and sand-producing zones in red. The sand production sensitivity analysis at 1819 mMD (Figure 5a) reveals that sanding occurs at this depth under any drawdown conditions. At 1821.7 mMD (Figure 5b), the formation remains sand-free throughout the entire life of the field.

Figure 5c presents the sensitivity analysis at 1823.15 mMD. Initially, at a reservoir pressure of 2589 psi (0% depletion) and a bottom hole pressure of 493 psi, the allowable drawdown pressure (DDP) to avoid sanding is 2096 psi. When the reservoir pressure depletes by 15% (to 2201 psi) with a corresponding bottom hole flowing pressure of 470 psi, the allowable DDP decreases to 1731 psi. At depletion levels of 30% and 35%, the allowable DDP should be limited to 1365 psi and 1235 psi, respectively. Finally, when the reservoir pressure declines to its critical depletion stage of 80% (starred point), the reservoir pressure drops to 516 psi while the bottom hole flowing pressure is 522 psi. At this stage, the well ceases to flow, and the wellbore faces a high risk of collapse under any applied drawdown.

In the perforated interval from 1817÷1823.6 mMD, the sand production prediction results show interbedded sanding and sand-free zones, indicating that sand production could occur under any drawdown condition. These results coincide with the sand samples observed at the surface during early production (Figure 5d). Table 2 shows the results of the sand production prediction for the perforated interval in the Miocene reservoir section.

4. Discussion

The results of sand production prediction for well A-1P show that intervals are prone to onset of sanding due to its lower mechanical strength

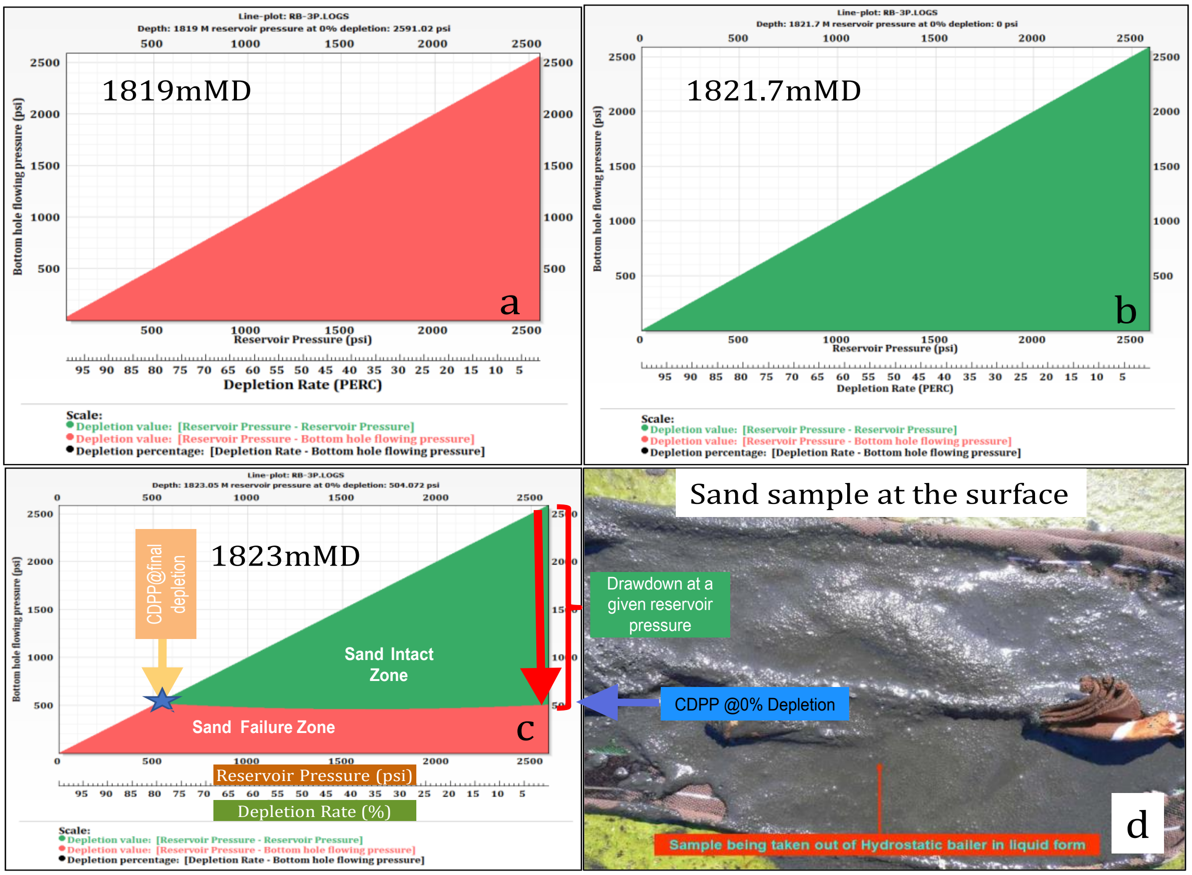

Figure 5. The sand production sensitivity analysis at depth of 1819mMD, 1821.7mMD, 1823mMD and sand count at the surface.

Table 2. Sand production prediction for production zone in well A-1P.

Depth (m)	UCS Log (psi)	UCS Core (psi)	TWC Log (psi)	TWC Core (psi)	σH (psi)	σh (psi)	Pore pressure (psi)	CDDP (0,15,30,35) (psi)	LF (0,30,60,90)	Prediction
1817	1611	2651	6306	6500	4344	3968	2411	1684; 1943; 2203; 2591	0.8; 0.8; 0.9; 0.9	Sand-free
1819	1850	1147	6075	4269	4412	3986	2412	197; 480; 753; 1147	1.1; 1.1; 1.3; 1.3	Sand
1819	1281		4731		4342	3959	2413	10; 20; 45; 75	1.3; 1.3; 1.5; 1.5	Sand
1820	3333		8732		4524	3986	2414	1683, 1942, 2201, 2950	0.7; 0.7; 0.8; 0.8	Sand-free
1822	3623		8373		4387	3965	2416	1683; 1942; 2201; 2589	0.7; 0.7; 0.8; 0.9	Sand-free
1822	3356		8875		4270	4003	2417	1683; 1942; 2201; 2589	0.7; 0.7; 0.8; 0.8	Sand-free
1823	3550	4919	8297	10114	4364	4092	2417	1683; 1942; 2201; 2589	0.7; 0.8; 0.9; 0.9	Sand-free
1823	2194		7791		4396	4314	2418	1225; 1479; 1726; 2085	0.8; 0.8; 1.1; 1.1	Sands occur @LF60, LF90

(low UCS or TWC). When subjected to differiential stresses, the stress concentration around the wellbore exceeds the shear failure envelope of the rock, initiating disaggration of sand grains even at low CDDP and regardless of perforation orientation (LF>1 from 0÷90^0). Conversely, these stable zones remain sand-free because they posses higher UCS and TWC values, reflecting better cohensive strength enables the perforation cavity walls to withstand higher shear stress concentrations caused by CDDP and perforation orientation. However, sand production occurs when perforation angle is above 60^0 due to higher shear concentrations to generate LF>1 and enabling sand production. Beside that, as reservoir pressure depletes, the pore pressure supporting for rock strength decreases, resulting in a increase in effective overburden and horizontal stresses according to Terzaghi's stress principle. Consequently, this process gradually weakens the cohension strength of wallbore, systematically reducing the allowable CDDP.

These results remain many uncertainties and limitations due to the lack of mechanical core tests for calibration with UCS and TWC log profile. Some cases, sand grains can not be transported to the surface and accumulated in the wellbore due to low flow rate, potentially leading to the false interpretation that no sand production has occurred. Therefore, it is essential to integrate well intervention data into the post well sand production prediction studies.

5. Conclusion

Sand production prediction modeling is not a new topic; however, previous studies have primarily addressed stress conditions at the wellbore scale, often overlooking the stress redistribution occurring around the walls of perforation tunnels. This study successfully developed a comprehensive geomechanical model for Well A-1P, targeting Miocene reservoirs in the Cuu Long Basin, which is characterized by a normal faulting stress regime.

The approach utilizes a cylindrical coordinate system to integrate the redistributed stress state around the perforation tunnel wall into a failure assessment based on the Load Factor (LF) criterion. Based on this theoretical framework, a Python-based numerical script was developed to solve complex stress equations across a 360^0 circumferential interval. Concurrently, a continuous thick-walled cylinder strength profile along the wellbore generated by using an empirical correlation between core laboratory tests and log-derived uniaxial compressive strength. These integrated parameters enable the precise calculation of LF for various perforation angles (0^o, 30^0, 60^0, 90^0) and the determination of reliable Critical Drawdown Pressures (CDDP) under reservoir depletion scenarios of 0%, 15%, 30%, and 35%.

For the perforated interval (1817÷1823.6 mMD), which produced 928 BOPD and 5.74 MMscf/day, the model identifies the depths of 1817.2÷1817.8 mMD, 1818.8÷1819.8 mMD, and 1820.6÷1820.8 mMD as high-risk zones. In these intervals, LF>1 and the allowable Drawdown Pressure (DDP) drops significantly, indicating that sanding is likely under most drawdown conditions.

These findings identify specific sand-prone intervals and provide a critical foundation for optimizing drawdown strategies and selecting effective sand-control completions for Miocene reservoirs. Furthermore, sand-prone intervals should be avoided during perforation, and the Critical Drawdown Pressure (CDP) must be dynamically managed to mitigate sanding risks during the late stages of reservoir depletion.

Contributions of authors

Hoang Van Nguyen - methodology, writing, review & editing; Huong Thien Phan, Vinh The Nguyen - critical review & supervision.

References

Asadi, M. S., Khaksar, A., Ring, M. J., Saric, D. & Yin Yin, M. (2016). Solids production prediction and management for oil producers in highly depleted reservoirs in a mature malaysian field. *Day 1 Mon, September* 26, 2016, D011S013R004. https://doi.org/10.2118/181583-MS.

Banerjee, A., Saha, S., Kidambi, T., Telang, V., Hunnur, A. & Khaksar, A. (2020). Geomechanical Sanding Analysis: Criticality in Testing and Sampling in Unconsolidated Formations - A Case History. *Day 1 Mon, November* 09, 2020, D012S116R083. https://doi.org/10.2118/203423-MS.

Binh, N. T. T., Tokunaga, T., Goulty, N. R., Son, H. P. & Van Binh, M. (2011). Stress state in the cuu long and nam con son basins, offshore vietnam. *Marine and Petroleum Geology*, 28(5), 973-979.

Binh, N. T. T., Tokunaga, T., Son, H. P. & Van Binh, M. (2007). Present-day stress and pore pressure fields in the Cuu Long and Nam Con Son Basins, offshore Vietnam. *Marine and Petroleum Geology*, 24(10), 607-615.

Ding, Y., Liu, X. & Luo, P. (2018). The analytical model of hydraulic fracture initiation for perforated borehole in fractured formation. *Journal of Petroleum Science and Engineering,* 162, 502-512. https://doi.org/10.1016/j.petrol.2017.10.008.

Ding (2017). The analytical model of hydraulic fracture initiation for perforated borehole in fractured formation. Elsevier, *Journal of Petroleum Science and Engineering*, 502-512. https://doi.org/https://doi.org/10.1016/j.pe trol.2017.10.008.

Dung, T. Q., Tung, H. T. (2014). The model to predict sand production for production wells at Cuu Long basin. *Science & technology developmen*, 17(5), 172-178.

Duyen, Q. L. (2024). Application of geomechanical models to predict sand production and propose well completion solutions for Well X in the Hai Thach field. *Journal of hydro-meteorology*. https://doi.org/10.36335/VNJHM.2024(20).75-83.

Fjaer, E., Holt, R. M., Horsrud, P. & Raaen, A. M. (2008). Petroleum related rock mechanics (Vol. 53). *Elsevier*.

Fuller, J., Cook, J. M., Subbiah, S. K., De Groot, L. & Graven, H. (2017). Balancing Productivity and Sanding Risk in Weak Sandstones Through a Size Dependent Approach. *ARMA*-2017-0600.

Hoang, V. N. (2026). Correlation between P-wave modulus (M) and Uniaxial compressive strength (UCS) derived from hydraulic flow units (HFU). *Journal of Mining and Earth Sciences,* 66(1). https://doi.org/10.46326/JMES.2026.67(1).08.

Khamehchi, E. & Reisi, E. (2015). Sand production prediction using ratio of shear modulus to bulk compressibility (case study). *Egyptian Journal of Petroleum*, 24(2), 113-118. https://doi.org/10.1016/j.ejpe.2015.05.002.

Rahman, K., Khaksar, A. & Kayes, T. (2010). An Integrated Geomechanical and Passive Sand-Control Approach to Minimizing Sanding Risk From Openhole and Cased-and-Perforated Wells. *SPE Drilling & Completion*, 25(02), 155-167. https://doi.org/10.2118/116633-PA.

Tran, Q. A. (2025). Determination of thick walled cylinder strength in sand control for production wells in Block 46, Malay-Tho Chu Basin. *Journal of Mining and Earth Sciences,* 66(5), 110-119.

Wang, H., Zhou, D., Liu, S., Wang, X., Ma, X. & Yao, T. (2022). Hydraulic fracture initiation for perforated wellbore coupled with the effect of fluid seepage. *Energy Reports*, 8, 10290-10298. https://doi.org/10.1016/j.egyr.2022. 08.011.

Waters, G. & Weng, X. (2016, September). The impact of geomechanics and perforations on hydraulic fracture initiation and complexity in horizontal well completions. *In SPE Annual Technical Conference and Exhibition*? (p. D031S042R002). *SPE*. https://doi.org/10.2118/181684-MS.

Willson, S. M., Z. A. Moschovidis, J. R. Cameron, and I. D. Palmer (2002). New model for predicting the rate of sand production. *SPE/ISRM Rock Mechanics ConferenceSPE*. http://dx.doi.org/10.2523/78168-MS.

Wu, B. ., Bahri, C. ., Tan, C. P., Li, Q. ., Rahim, H. ., Kartoatmodjo, G. . & Friedel, T. (2010). Sand Production Prediction for a Mature Oil Field Offshore East Malaysia-A Case Study. *All Days*, SPE-133375-MS. https://doi.org/10.2118/133375-MS.

Zain-Ul-Abedin, M. & Henk, A. (2020). Building 1D and 3D mechanical earth models for underground gas storage-A case study from the Molasse Basin, *Southern Germany. Energies*, 13(21), 5722.

Zoback, M. D. (2007). Reservoir Geomechanic. *Cambridge University Press.* www.cambridge.org/9780521770699.